ARTICLE NO. 79-0585R

C80-077

Finite Element Subvolume Technique for Structural-Borne Interior Noise Prediction

00013
00023
30003

J. F. Unruh*
Southwest Research Institute, San Antonio, Texas

Finite element structural and acoustic representations of a vibrating structure and enclosed acoustic volume are used in a study of structural-borne interior noise. The direct finite element nodal representations of the equations of motion result in a large system of unsymmetric equations. In this paper, an acoustic subvolume analysis technique is presented which reduces the degrees of freedom of the interior volume to modal form prior to the coupled system dynamic analysis. Analytical predictions are compared to results from an experimental program to verify the analysis procedures. From these comparisons, the acoustic subvolume technique is shown to be a reliable method to reduce the computational requirements for finite element acoustic analysis.

Nomenclature

A = subscript denoting acoustic region
$A(\omega)$ = acoustic admittance, frequency dependent
B = a product of two matrices defined in Eq. (27)
$C_A(\omega)$ = acoustic damping matrix, frequency dependent
C_S = structural damping matrix
c = speed of sound in the acoustic media
F = externally applied structural forces
$\bar{F}$ = generalized applied forces
I = subscript or superscript denoting interior region and unit diagonal matrix
i,j = indices
K = stiffness matrix, in general
M = mass matrix, in general
N = number of basis functions
P = nodal perturbation pressure, in general
$\hat{P}_I$ = interior pressures for zero surface pressures
p = acoustic perturbation pressure
Q = eigenvectors, in general
q_A = acoustic subvolume modal degrees of freedom
q_S = structural modal degrees of freedom
R = applied structural loads or acoustic region
r = a subscript denoting rth coupled mode
S = transformed stiffness matrix or surface of acoustic region; also subscript or superscript denoting surface nodes
T = decoupling transformation submatrix
t = temporal variable
u = structural nodal displacements
W = transformed mass matrix
β = logarithmic damping ratio
γ = coupled system modal degrees of freedom
η = outward normal to the boundary
λ = eigenvalue, square of the circular frequency
ρ_0 = mean density of the acoustic media
ϕ_j = jth pressure series basis function
ψ = coupled system eigenvectors
ω = circular frequency
∇ = gradient operator
∇^2 = Laplacian operator

Presented as Paper 79-0585 at the AIAA 5th Aeroacoustics Conference, Seattle, Wash., March 12-14, 1979; submitted March 22, 1979; revision received June 22, 1979.

Index categories: Analytical and Numerical Methods; Noise; General Aviation.

*Senior Research Engineer, Department of Mechanical Sciences. Member AIAA.

Introduction

INTERIOR noise levels in general aviation propeller-driven aircraft are often higher than those considered marginally acceptable in other forms of transportation. The noise spectra of these aircraft are dominated by a series of low-frequency components which are harmonics of the engine and propeller. Airborne propeller noise and structure-borne engine vibration transmission appear to be the major sources of noise.[1-4] Effective noise control at the airframe design level or via airframe modification will require reliable interior noise prediction procedures. However, methods for predicting interior noise levels due to structure-borne vibration and sidewall transmission in geometrically complex enclosures are not readily available,[5] particularly in the low-frequency region wherein the acoustic modal density is very low and methods of architectural acoustics do not apply. Classical acoustic modal solution methods via continuous function representation are generally limited to variable separable geometries. Examples of continuous function solutions are given by Cockburn and Jolly[6] for a cylindrical fuselage model and by Vaicaitis and McDonald[7] for a rectangular fuselage model. The modal approach can be extended to nonvariable separable geometries via the method of weighted residuals (MWR)[8]; however, therein persists the problem of choosing a set of complete functions for the modal expansion throughout the volume and carrying out the detailed integrations pertaining to the given fuselage geometry. To avoid these problems while possibly increasing computational efforts, the direct approach of constructing the fuselage volume from a series of acoustic finite elements would appear to be a more workable approach.

The acoustic finite element representation for interior noise studies has received considerable attention in the past few years. Initial work focused on developing acoustic finite elements and computing resonant frequencies of complex-shaped enclosures.[9-12] Thereafter, some effort was given to the study of acoustic volumes excited by flexible boundaries.[13] Most recently, Nefske and Howell[14] describe an application of acoustic finite element analysis using NASTRAN to reduce automobile low-frequency interior noise. The finite element approach has also been extended to modeling cavities with absorbing boundaries[15-17] for studies of impedance models and muffler design.

In the present investigation, finite element structural and finite element acoustic representations of a flexible structure

and receiving acoustic volume are used to formulate the equations of motion for a coupled structural acoustic system. While similar approaches have been used by others, in the previous studies the coupled structural acoustic system of equations was solved directly from the nodal representations which resulted in a rather large system of unsymmetric equations. In the present study, the number of system coupled equations are reduced prior to forced harmonic response analysis by expanding the structural equations of motion in terms of their normal mode eigenvectors, and the interior acoustic nodal equations are reduced to modal form via an acoustic subvolume technique. In this manner, the final coupled equations are cast in terms of modal degrees of freedom of the structure and interior acoustic field and nodal degrees of freedom of the surface nodes. The acoustic subvolume technique is an application of a fixed-interface[18] method of substructuring using constraint modes. The subvolume technique will be shown to apply to a wide variety of acoustic formulations.

In the sections to follow, the basic equations of motion of the coupled structural-acoustic system will be given along with the mathematical procedures associated with the acoustic subvolume technique used to transform the interior acoustic volume into a modal representation. Thereafter, an experimental program is described from which normal mode frequencies and forced harmonic response data were obtained and used for comparison to analytical results generated using the subvolume analysis technique.

Equations of Motion

Structural Equations

The finite element method is well known for its application in structural analysis. For the details on structural element generation and solution methods, reference is made to the work of Przemieniecki[19] and Zienkiewicz.[20] In general, we may write the dynamic structural equations of motion in matrix form as

$$[M_S]\{\ddot{u}\}+[C_S]\{\dot{u}\}[K_S]\{u\}=\{R\} \tag{1}$$

where M_S, C_S, and K_S are the assembled nodal mass, damping, and stiffness matrices for the structure and u are the nodal degrees of freedom. The applied loads consist of two terms, namely,

$$\{R\}=[K_{SA}]\{P_S\}+\{F\} \tag{2}$$

The first term in Eq. (2) represents the applied forces due to the acoustic back pressure which is a function of the nodal surface pressures P_S, and the second term F are the externally applied forces to the structure.

Acoustic Equations

The acoustic equations of motion are developed from the small perturbations source free wave equation,[21]

$$\nabla^2 p-1/c^2\ddot{p}=0 \tag{3}$$

where p is the perturbation pressure, c is the speed of sound in the media, and ∇^2 is the Laplacian operator. On the boundaries of the acoustic region, the governing equations are subject to various boundary conditions:

1) At a rigid boundary

$$\partial p/\partial\eta=0 \tag{4}$$

where η is the outward normal to the boundary;

2) At a vibrating boundary

$$\partial p/\partial\eta=-\rho_0\ddot{u} \tag{5}$$

where $\ddot{u}$ is the acceleration normal to the boundary, and ρ_0 is the mean density of the acoustic media;

3) At an absorptive boundary

$$\partial p/\partial\eta=-\rho_0 A(\omega)\dot{p} \tag{6}$$

where $A(\omega)$ is acoustic admittance of the boundary which is assumed to be frequency-dependent and, therefore, implies that p exhibits an harmonic time dependence [$p=\bar{p}\exp(i\omega t)$].

The absorptive boundary condition is included in the general derivations herein because of its importance to noise control investigations and to point out the usefulness of the subvolume approach for investigations using boundary absorptive elements as well. However, no analytical or experimental work with absorptive boundaries is presented in this paper.

If we expand the pressure in terms of a series of basis (shape) functions, we may write

$$p=\sum_{j=1}^{N}\phi_j P_j \tag{7}$$

where $\phi=\phi_j(x,y,z)$ characterizes the spatial dependence of p and $P_j=P_j(t)$, the temporal dependence.

Upon substitution of the assumed pressure series into the equations of motion, a distribution of errors results throughout the acoustic region due to the general nature and finiteness of the assumed pressure series. In accordance with the method of weighted residuals,[8] we force the distribution of errors to be orthogonal within the region to each of the basis functions in the expansion. Thus,

$$\int_R \phi_i[\nabla^2 p-1/c^2\ddot{p}]\,dR=0,\ \text{for } i=1,2,3\ldots N \tag{8}$$

By making use of Green's vector identity,

$$\phi_i\nabla^2(p)=-\nabla(\phi_i)\cdot\nabla(p)+\nabla\cdot(\phi_i\nabla(p)) \tag{9}$$

and the integral form of the divergence theorem of Gauss,

$$\int_R \nabla\cdot(\phi_i\nabla_p)\,dR=\int_S \phi_i\nabla p\cdot\eta\,dS \tag{10}$$

where R is the acoustic region, S its bounding surface and η the outward normal to the region,[22] the acoustic equations of motion become

$$\frac{1}{c^2\rho_0}\sum_{j=1}^{N}\int_R \phi_i\phi_j\,dR\ddot{P}_j+\frac{1}{\rho_0}\sum_{j=1}^{N}\int_R\left\{\frac{\partial\phi_i}{\partial x}\frac{\partial\phi_j}{\partial x}+\frac{\partial\phi_i}{\partial y}\frac{\partial\phi_j}{\partial y}+\frac{\partial\phi_i}{\partial z}\frac{\partial\phi_j}{\partial z}\right\}dR P_j=\frac{1}{\rho_0}\int_S\phi_i\frac{\partial p}{\partial\eta}\,dS,\ \text{for } i=1,2,3\ldots N \tag{11}$$

The first term on the left is referred to as the acoustic mass, the second term the acoustic stiffness, and the right-hand side the applied boundary forces. Here we note that the constant $1/\rho_0$ has been added to the equations for purposes of dimensionality, and the term $\partial p/\partial\eta$ has not been expanded into its series form to allow direct substitution of the boundary equations, Eqs. (4), (5), and/or (6). As can be seen for a hard wall boundary, there are no applied forces whereas for a vibrating boundary, the applied forces are proportional to the boundary acceleration; for an absorptive boundary, the boundary forces appear as damping terms, i.e., proportional to $\dot{P}_j$. The above formulation of the acoustic equations of motion are valid for the entire acoustic region R or any

subregions within R, or on its surface. Thus, we can see that by letting R represent the region of a single acoustic finite element and S the surface of that element, we may easily discretize the region into an assemblage of finite elements. Reference is made to the work of Zienkiewicz for the various basis (shape) functions that can be used for the acoustic element generation, which are essentially the same as those used in the generation of structural finite elements.

The assembled matrix form of the acoustic equations of motion is

$$\begin{bmatrix} M_A{}^{SS} & M_A{}^{SI} \\ M_A{}^{IS} & M_A{}^{II} \end{bmatrix} \begin{Bmatrix} \ddot{P}_S \\ \ddot{P}_I \end{Bmatrix} + \begin{bmatrix} C_A{}^{(\omega)} & 0 \\ 0 & 0 \end{bmatrix} \begin{Bmatrix} \dot{P}_S \\ \dot{P}_I \end{Bmatrix} + \begin{bmatrix} K_A{}^{SS} & K_A{}^{SI} \\ K_A{}^{IS} & K_A{}^{II} \end{bmatrix} \begin{Bmatrix} P_S \\ P_I \end{Bmatrix} = \begin{bmatrix} -M_{AS} \\ 0 \end{bmatrix} \{ \ddot{u} \} \tag{12}$$

where M_A, C_A, and K_A are the acoustic mass, damping, and stiffness matrices, and M_{AS} is the inertia coupling associated with the boundary motion. The pressure nodal degrees of freedom are partitioned into those nodes on the surface P_S wherein damping or boundary motion is present and all other degrees of freedom which are referred to as interior nodes P_I.

Method of Solution

The structural equations of motion are reduced to modal form by expansion of the nodal displacements in terms of the structures normal mode eigenvectors.[23] The system normal mode eigenvectors are determined from the undamped homogeneous equations

$$[M_S]\{\ddot{u}\} + [K_S]\{u\} = 0 \tag{13}$$

via the equivalent linear eigenvalue problem

$$[K_S - \lambda M_S]\{u\} = \{0\} \tag{14}$$

where $\lambda = \omega^2$, the square of the normal mode frequencies. The physical displacements are related to the modal degrees of freedom q_S via the eigenvectors Q_S as

$$\{u\} = [Q_S]\{q_S\} \tag{15}$$

The eigenvectors are normalized such that they diagonalize the mass matrix to unity and the stiffness matrix to the square of the modal frequencies. The damping matrix is now chosen to be proportional to the system mass or stiffness, or linear combination of the two and, therefore, also assumes a diagonal form. This procedure transforms the structural nodal equations into the modal form:

$$[I]\{\ddot{q}_S\} + [2\beta\omega_S]\{\dot{q}_S\} + [\omega_S{}^2]\{q_S\} = [Q_S{}^T][K_{SA}]\{p_S\} + [Q_S{}^T]\{F\} \tag{16}$$

Here we note that for most practical problems, this modal expansion substantially reduces the number of structural equations since only those modal degrees of freedom whose normal mode frequencies lie within the analysis range of interest need to be retained. This method of reduction is commonly referred to as modal truncation or synthesis.

A direct expansion of the acoustic equations of motion in terms of the system normal cavity modes is not possible as was carried out for the structural equations. The normal mode expansions with $\partial p/\partial \eta = 0$ on the boundary would not allow representation of system absorption or forced vibration, since these inputs require nonzero boundary motion. However, in many problems the number of interior nodes plus surface nodes with negligible absorption or motion can be large as compared to those surface nodes that exhibit significant motion or absorptive capability. For these cases it would be advantageous to expand those interior nodes and surface nodes for which $\partial p/\partial \eta = 0$ into modal form and apply modal truncation to reduce the number of active degrees of freedom in the acoustic equations of motion.

This is accomplished by seeking a transformation that will stiffness-decouple the two coordinate sets. This transformation is

$$\begin{Bmatrix} P_S \\ P_I \end{Bmatrix} = \begin{bmatrix} I & 0 \\ T & I \end{bmatrix} \begin{Bmatrix} P_S \\ \hat{P}_I \end{Bmatrix} \tag{17}$$

where

$$[T] = -[K_A{}^{II}]^{-1}[K_A{}^{IS}] \tag{18}$$

The vectors of the transformation to the left of the partition are component modes of constraint. They represent the pressure perturbations at P_I when the constraint nodes P_S are individually given a unit pressure perturbation. It is to be noted that the node set P_I has been replaced with the set $\hat{P}_I$, which denotes the pressure perturbation of P_I when $P_S = 0$.

Substituting the transformation given in Eq. (17) into the acoustic Eq. (12), while simultaneously conserving system energy, results in the following equations of motion:

$$\begin{bmatrix} W_A{}^{SS} & W_A{}^{SI} \\ W_A{}^{IS} & M_A{}^{II} \end{bmatrix} \begin{Bmatrix} \ddot{P}_S \\ \ddot{\hat{P}}_I \end{Bmatrix} + \begin{bmatrix} C_A(\omega) & 0 \\ 0 & 0 \end{bmatrix} \begin{Bmatrix} \dot{P}_S \\ \dot{\hat{P}}_I \end{Bmatrix} + \begin{bmatrix} S_A{}^{SS} & 0 \\ 0 & K_A{}^{II} \end{bmatrix} \begin{Bmatrix} P_S \\ \hat{P}_I \end{Bmatrix} = \begin{bmatrix} -M_{AS} \\ 0 \end{bmatrix} [Q_S] \{\ddot{q}_S\} \tag{19}$$

where

$$W_A{}^{SS} = M_A{}^{SS} + T^T M_A{}^{IS} + M_A{}^{SI} T + T^T M_A{}^{II} T$$

and

$$W_A{}^{SI} = (W_A{}^{IS})^T = M_A{}^{SI} + T^T M_A{}^{II}$$

$$S_A{}^{SS} = K_A{}^{SS} + T^T K_A{}^{IS} \tag{20}$$

Here we note that the acoustic interior nodal mass and stiffness submatrices $M_A{}^{II}$ and $K_A{}^{II}$, and surface damping matrix $C_A(\omega)$, remain unchanged under this transformation and the degrees of freedom P_S and $\hat{P}_I$ have been stiffness-decoupled. The applied loads due to boundary motion also remain unchanged.

With the equations of motion in this form, we can again make use of the concept of model truncation by extracting the eigenvalues and eigenvectors for the subvolume consisting of the coordinate set $\hat{P}_I$ when it is subject to the constraint conditions $P_S = 0$. The resulting homogeneous equations of motion corresponding to this condition are

$$[M_A{}^{II}]\{\ddot{\hat{P}}_I\} + [K_A{}^{II}]\{\hat{P}_I\} = \{0\} \tag{21}$$

which has an associated linear eigenvalue problem of the same form as that given in Eq. (14) for the structural equations. Solution to the eigenvalue problem yields an associated set of eigenvectors or mode shapes

$$\{\hat{P}_I\} = [Q_A]\{q_A\} \tag{22}$$

normalized such that

$$Q_A{}^T M_A{}^{II} Q_A = I \text{ and } Q_A{}^T K_A{}^{II} Q_A = \omega_A{}^2 \tag{23}$$

where $\omega_A{}^2$ denotes a diagonal matrix of the squares of the circular frequencies arranged in an increasing order of magnitude. At this point, we may truncate the number of eigenvalues to be retained for representation of the subvolume. The number of modes retained in the expansion can generally be set to less than 30% of the original degrees of freedom set, thereby substantially reducing the total order, or degrees of freedom, of the system.

The reduced equations of motion for the coupled structural-acoustic system are

$$\begin{bmatrix} I & 0 & 0 \\ M_{AS}Q_S & W_A{}^{SS} & W_A{}^{SI}Q_A \\ 0 & Q_A{}^T W_A{}^{IS} & I \end{bmatrix} \begin{Bmatrix} q_S \\ P_S \\ q_A \end{Bmatrix} + \begin{bmatrix} 2\beta\omega_S & 0 & 0 \\ 0 & C_A(\omega) & 0 \\ 0 & 0 & 0 \end{bmatrix} \begin{Bmatrix} \dot{q}_S \\ \dot{P}_S \\ \dot{q}_A \end{Bmatrix} + \begin{bmatrix} \omega_S{}^2 & -Q_S{}^T K_{SA} & 0 \\ 0 & S_A{}^{SS} & 0 \\ 0 & 0 & \omega_A{}^2 \end{bmatrix} \begin{Bmatrix} q_S \\ P_S \\ q_A \end{Bmatrix} = \begin{Bmatrix} Q_S{}^T F \\ 0 \\ 0 \end{Bmatrix} \tag{24}$$

where the structural nodal motion is found from the expression given in Eq. (15), the interior nodal pressures are determined from

$$\{P_I\} = [T]\{P_S\} + [Q_A]\{q_A\} \tag{25}$$

and the surface pressures are directly P_S.

It is important to note that in the above procedure, the modal solution for the structural system is carried out independent from the acoustic problem. This requires that the acoustic back pressure be small in comparison to the structural stiffness. This will be the case so long as the lowest structural mode frequency is no lower than approximately 0.5 times the lowest acoustic cavity mode frequency.[9] For air, the mass loading of the structure by the acoustic volume will be negligible.

In the case of low-frequency noise generation, the acoustic absorption of the aircraft interior trim is generally negligible—in which case, the absorptive term $C_A(\omega)$ can be set to zero. The coupled structural-acoustic normal modes may be found from the homogeneous coupled equations. However, the homogeneous equations must first be placed into symmetric form if eigenvalue solutions are to be obtained using standard eigenvalue extraction routines. The equations in symmetric form are

$$\begin{bmatrix} \omega_S{}^2 & 0 & 0 \\ 0 & W_A{}^{SS} & W_A{}^{SI}Q_A \\ 0 & Q_A{}^T W_A{}^{IS} & I \end{bmatrix} \begin{Bmatrix} \ddot{q}_S \\ \ddot{P}_S \\ \ddot{q}_A \end{Bmatrix} + \begin{bmatrix} \omega_S{}^4 & [\omega_S{}^2][B] & 0 \\ -[B^T][\omega_S{}^2] & S_A{}^{SS} + B^T B & 0 \\ 0 & 0 & \omega_A{}^2 \end{bmatrix} \begin{Bmatrix} q_S \\ P_S \\ q_A \end{Bmatrix} = \begin{Bmatrix} 0 \\ 0 \\ 0 \end{Bmatrix} \tag{26}$$

where

$$B = Q_S{}^T K_{SA} \tag{27}$$

Solution of the corresponding eigenvalue problem results in an associated set of eigenvectors

$$\begin{Bmatrix} q_S \\ P_S \\ q_A \end{Bmatrix} = [\psi] \quad \{\gamma\} = \begin{Bmatrix} \psi_{SS} \\ \psi_{AS} \\ \gamma_{AA} \end{Bmatrix} \{\gamma\} \tag{28}$$

which are used to diagonalize the original nonhomogeneous system of equations, resulting in

$$[M]\{\ddot{\gamma}\} + [2\beta\omega_{SA}]\{\dot{\gamma}\} + [\omega^2{}_{SA}]\{\gamma\} = \{\bar{F}\} \tag{29}$$

where

$$\{\bar{F}\} = [\psi^T] \begin{bmatrix} \omega_S{}^2 \\ B^T \\ 0 \end{bmatrix} \{Q_S{}^T F\} \tag{30}$$

Solution to the diagonalized system for forced harmonic input is

$$\gamma_r = \frac{\bar{F}_r(\omega)}{(\omega^2{}_{SA} - \omega^2) + i2\beta\omega_{SA}\omega} \tag{31}$$

where r denotes the rth coupled mode and γ_r the response in that mode; Eqs. (15), (19), and (25) then specify the nodal responses. Some liberty has been taken in Eq. (29) insofar as including a diagonalized damping matrix, since the diagonalized structural damping matrix will not be rediagonalized by the coupled mode vectors. However, as will be shown in the example to follow, the diagonal modal damping representation is a good approximation for lightly damped systems. It should be pointed out that the coupled system eigenvalues have a single zero frequency which corresponds to a constant pressure throughout the acoustic volume.

Since the computational effort for eigenvalue extraction is approximately dependent on the cube of the degrees of freedom of the system, it can be seen that the application subvolume technique for even hardwall normal mode eigenvalue extraction can result in considerable savings in computational effort. One may also consider multiple application of the subvolume technique for larger problems by subdividing the interior region into a number of subvolumes. For this case, the interface nodes between interior subvolumes would initially appear as surface nodes which thereafter could be reduced to modal form as well.

Experimental Program

A test fixture was designed and built to experimentally obtain hardwall acoustic modes, coupled structural-acoustic modes, and interior sound pressure levels for forced harmonic input in a geometrically complex-shaped enclosure. Results from these tests were then used to compare to analytical results generated using the acoustic subvolume analysis technique. A schematic of the test fixture and its inside dimensions are shown in Fig. 1. The interior depth of the fixture is 8.0 in. The basic construction consisted of 3/4-in. plywood sides with ¼-in. × 2-in. × 2-in. angle iron stiffeners which provided attachment for all side walls to the 1.0-in. plywood base. The base was externally reinforced with a series of 2-in. × 4-in. stiffeners. The 1.0-in. plexiglass top was reinforced with four vertical ⅜-in. rods attached to the base to minimize drumlike response. The 20-in. end of the fixture at $Y=0$ was fitted with an interchangeable end panel. For a

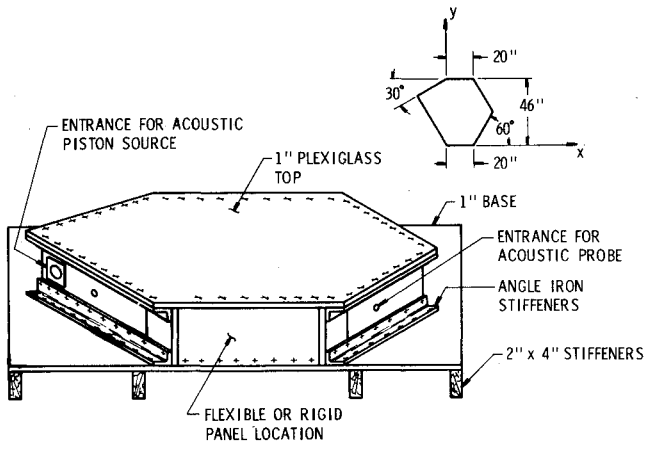

Fig. 1 Test fixture schematic and dimensional data.

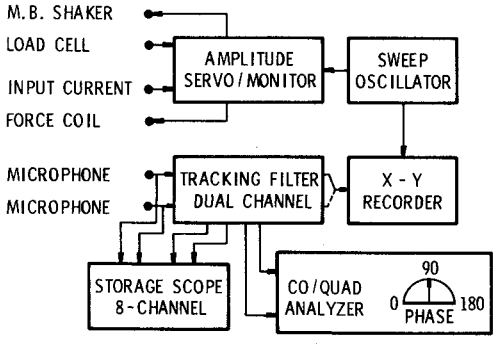

Fig. 2 Instrumentation and data acquisition system.

series of the tests, the end panel was rigid, made from ¾-in. plywood. The flexible end panel was a ⅛-in. × 8-in. × 20-in. aluminum plate clamped along the 8-in. dimension and free along the 20-in. dimension. The flexible panel was mass loaded with two 1.06 oz lumped masses at $X=8.0$ and 12.0 in. on center along the panel to account for the mass loading of the force coil armature.

A 2-in. diam piston attached to an electrodynamic shaker provided acoustic excitation during the tests. The test fixture was fitted with three input locations for the acoustic piston source. With the flexible panel installed, a force coil was attached along the center of the flexible panel at $X=12.0$ in. to provide structural excitation during the harmonic response tests.

A probe fitted with a ¼-in. microphone was used to survey the interior of the acoustic space via entrance from a series of ports (¾-in. holes) placed about the centerline of the test fixture. One additional surface mounted reference microphone was located at an adjacent port to act as a phase reference. Acoustic normal modes were determined by sweeping the frequency range of interest until both surface and interior microphones showed simultaneous peak response (except at acoustic nodes), indicating a resonant condition within the acoustic volume. At this point the node lines of the mode were mapped via the instrumentation setup shown in Fig. 2. Outputs from the two microphones were input into a narrow band (2 Hz) tracking filter, then routed to a CO/QUAD analyzer. In theory, as the traversing microphone passes through a node line, the phase would immediately shift 180 deg. However, in reality, dissipation in the system gives rise to a finite node width through which the phase will change continuously. Thus, by observing the relative phase of the two microphones, positions of the node lines were recorded at phase shifts of 90 deg.

Modal decays of the resonances were recorded by direct storage of the decay signal as the input was abruptly turned

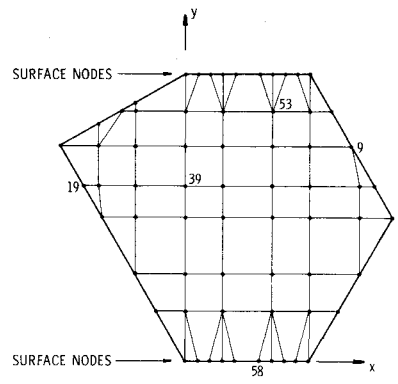

Fig. 3 Finite element model of the test fixture—Model B.

off. For these records the microphone outputs were input directly into the storage scope, which was triggered by turning off the input source. Logarithmic decrement damping ratios were then obtained from the decay traces using

$$\beta = \ln (A_0/A_N)/2\pi N \tag{32}$$

where A_0 is the initial amplitude of the oscillation and A_N is the final amplitude after N cycles.

Forced harmonic response sweeps were recorded for a constant force input by maintaining a constant current into the force coil via an amplitude servo/monitor. As seen in Fig. 2, a sweep oscillator was used to drive the amplitude servo/monitor and the X-axis of an X-Y recorder. The microphone output was then used to drive the Y-axis of the recorder. For the results presented below, the sweep oscillator was initially set at 20 Hz with a sweep rate of 0.1 decade/min. The slow sweep rate insured accurate peak responses throughout the recorded frequency range.

Comparison of Results

Analytical hardwall modes were computed for the test fixture geometry based on a speed of sound of 13,500 in./s. With the depth of the test fixture being 8.0 in., the response of the acoustic volume was considered two-dimensional since the recorded frequency range was reasonably below the first vertical mode resonance at 844 Hz. Two finite element models were initially used to analyze the hardwalled configuration. Model A consisted of 113 nodal degrees of freedom with 114 acoustic finite elements. Model B consisted of 66 nodal degrees of freedom with 59 acoustic finite elements, as is shown in Fig. 3. The finite elements used in the models were developed based on area coordinates[19] as the basis functions for the element expansions. Model A was only used initially to numerically check the accuracy obtained with Model B. The solution of Model A consisted of a full analysis wherein a 113 degrees of freedom eigenvalue analysis was carried out directly. A subvolume analysis was performed on Model B using the 10 nodes along $Y=0.0$ and the 10 nodes along $Y=46.0$ in. as surface nodes P_S and the remaining 46 nodes as interior nodes P_I. In the Model B analysis, 18 constraint mode degrees of freedom were retained from the subvolume analysis. Thus, in the Model B analysis, the subvolume procedure reduced computational time on the order of $(46/66)^3 + (38/66)^3 = 50\%$ of that required for a full anlaysis at 66 degrees of freedom. All computations were performed on a CDC 6600 computer from a FORTRAN source program.

Frequencies and node line plots from the Model A and Model B analyses are given in Fig. 4 and are compared to the experimental results for the first six hardwalled acoustic modes. As can be seen, both Model A and Model B yield acceptable results when compared to the test data; however, in general, Model A shows somewhat better correlation to the

Table 1 Summary of results

Coupled mode no.	Panel alone		Hardwalled[a]			Flexible panel installed			Panel and box[b] from sweeps
	Analytical	Experimental	Frequency Analytical	Frequency Experimental	Damping β	Frequency Analytical	Frequency Experimental	Damping β	
1	68.	68.				69.	73.	0.0048	73.
2			158.	155.	0.0087	159.	159.	0.0111	159.
3			181.	179.	0.0057	179.	183.	0.0076	177.
4	180.	183.				182.	190.	0.0014	190.
5			271.	262.	0.0140	271.	266.	0.0122	262.
6			305.	293.	0.0164	305.	296.	0.0090	296.
7			361.	350.	0.0117	361.	351.	0.0159	348.
8			396.	374.	0.0063	395.	375.	0.0082	377.

[a] Acoustic piston source. [b] Force coil panel source.

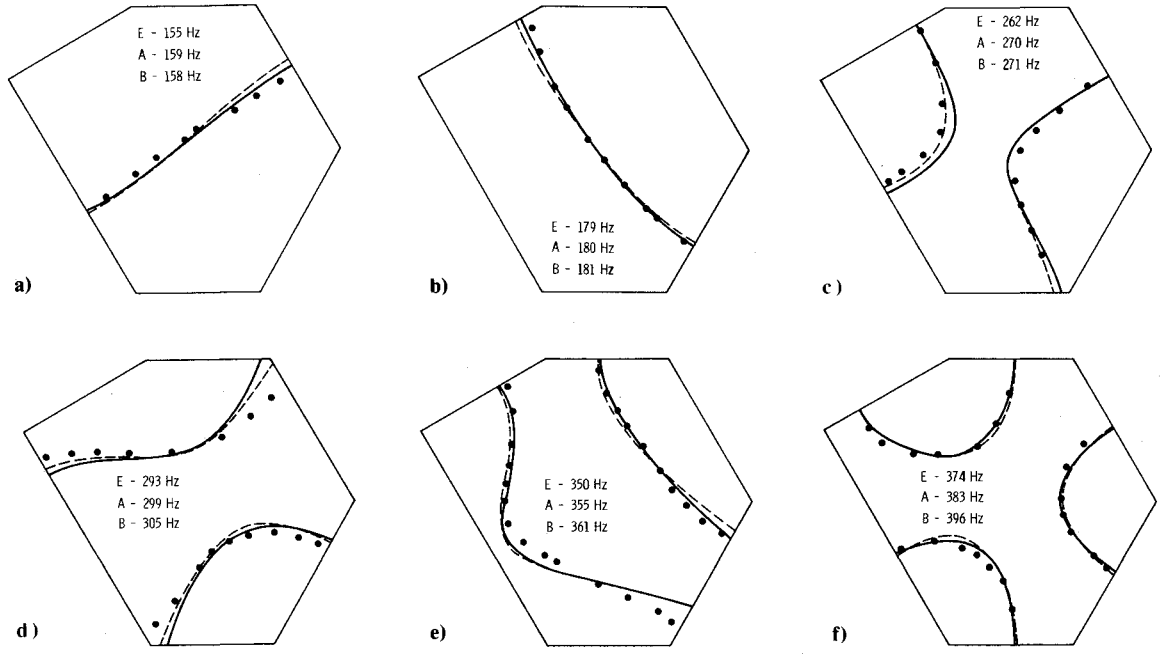

Fig. 4 Test fixture hardwalled frequencies and node lines: • and E, experimental;—and A, Model A (114 elements); -- and B, Model B (66 elements).

experimental results which should be expected from the more detailed model. At this point in the program, the accuracy given by Model B was determined to be sufficient and Model A was no longer exercised. A summary of the computed and measured resonant frequencies and corresponding logarithmic modal damping ratios are given in Table 1. Note that the mode numbering given in Table 1 for the hardwalled configuration is referenced to the corresponding coupled modes obtained for the flexible panel case, which is discussed below.

The flexible panel mounted in its test fixture hardware exhibited first and second mode frequencies of 68 and 180 Hz, respectively. For these tests, the panel was not connected to the acoustic volume. The end panel was analytically modeled as a series of 9 beam elements with nodes at corresponding locations to those shown in Fig. 3 for the acoustic model. The structural analysis resulted in resonant frequencies at 68 and 183 Hz.

In Fig. 5, experimental and computed frequencies and node line plots are given for the first eight coupled structural-acoustic resonances resulting from installation of the flexible end panel. The coupled frequencies and damping ratios are also listed in Table 1. Overall, the computed frequencies and mode shapes compare well to the experimental results. As can be seen by comparison of data presented in Table 1, the flexible panel increased the acoustic modal damping of mostly all of the equivalent hardwalled modes, the only exceptions being Modes 5 and 6. The decrease in damping for Mode 5 is explained as being within the expected experimental accuracy; however, the large reduction for Mode 6 is not as easily explained. As will be seen in the sweep data discussed in the following paragraph, the coupled mode value at 0.009 appears to be correct based on the analytical results obtained using this value of damping. Thus, the relatively high hardwalled damping value for Mode 6 appears to be in error.

Microphone sound pressure levels (SPL) within the test fixture were recorded while a force coil, attached to the flexible panel at node 58, provided harmonic input excitation from 20 to 400 Hz. The force coil output was maintained at a constant 0.12 lb force throughout the sweep. Corresponding forced harmonic response analyses were carried out using the computed coupled modes and experimentally determined damping values given in Table 1. Typical measured and computed sound pressure levels for surface mounted microphones are given in Figs. 6 and 7, corresponding to outputs at acoustic nodes 9 and 19. Likewise, interior SPL responses are given in Figs. 8 and 9, corresponding to interior positions at acoustic nodes 39 and 53. In general, the peak

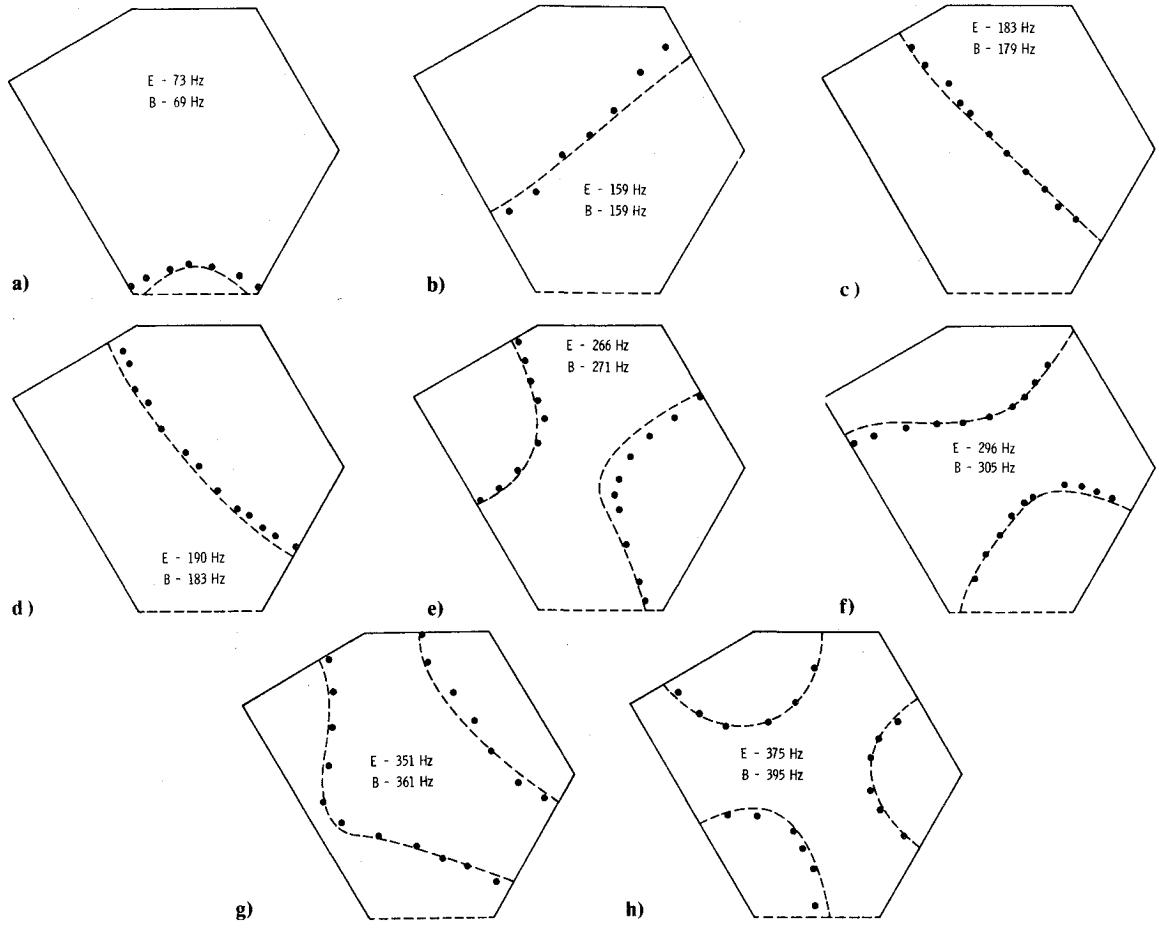

Fig. 5 Test fixture with flexible panel frequencies and node lines: • and E, experimental; -- and B, Model B.

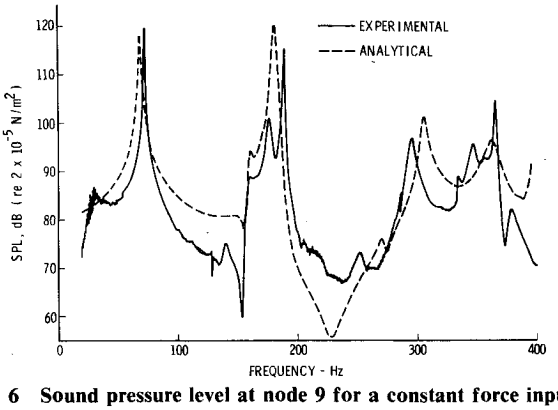

Fig. 6 Sound pressure level at node 9 for a constant force input of 0.12 lb_f rms on flexible panel at node 58.

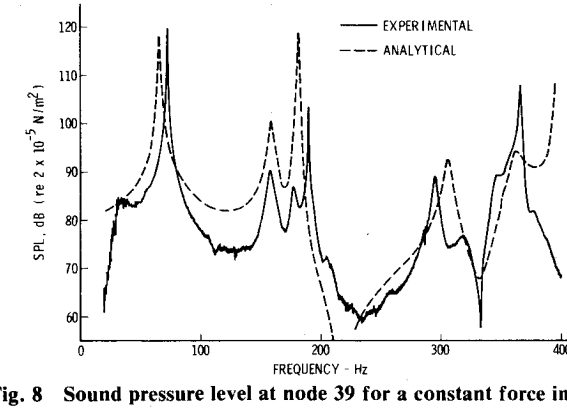

Fig. 8 Sound pressure level at node 39 for a constant force input of 0.12 lb_f rms on flexible panel at node 58.

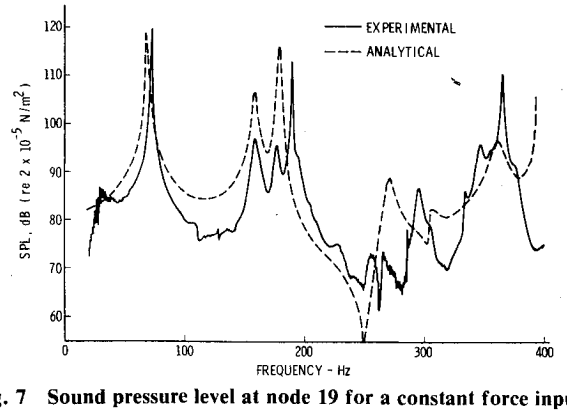

Fig. 7 Sound pressure level at node 19 for a constant force input of 0.12 lb_f rms on flexible panel at node 58.

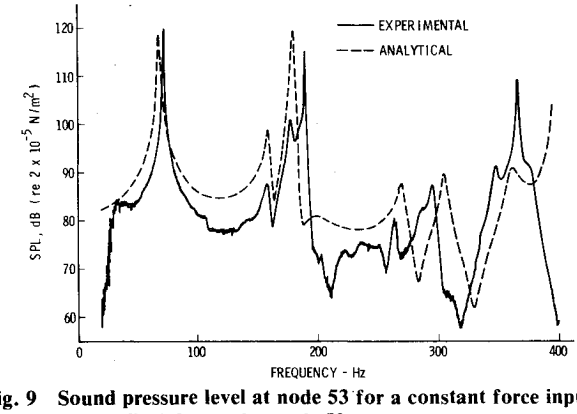

Fig. 9 Sound pressure level at node 53 for a constant force input of 0.12 lb_f rms on flexible panel at node 58.

responses of lower frequency modes are quite well predicted; however, as the frequency is increased the spread in modal frequency becomes more apparent. As can be seen, the panel resonances at 73 and 180 Hz dominate the acoustic response as would be expected for direct excitation of the panel.

Concluding Remarks

An acoustic subvolume analysis technique has been developed to reduce the computational effort required for finite element acoustic analyses. Through comparison with experimental results, the method has been shown to be an accurate analysis tool for the prediction of structure-borne noise. It appears that the subvolume analysis can also be used to reduce computational efforts in studies where acoustic boundary absorption is of interest. Work is presently under way using the acoustic subvolume analysis technique to study the structure-borne noise characteristics of a single engine general aviation aircraft. Preliminary results of this work are given in Ref. 24.

Acknowledgment

The author wishes to thank D. C. Scheidt for assistance given during the experimental phase of the program. This work was supported by Southwest Research Institute Internal Research Program.

References

[1] Catherines, J.J. and Mayes, W.H., "Interior Noise Levels of Two Propeller-Driven Light Aircraft," NASA TM X-72716, July 1975.

[2] Catherines, J.J. and Jha, S.K., "Source and Characteristics of Interior Noise in General Aviation Aircraft," NASA TM X-72839, April 1976.

[3] Jha, S.K. and Catherines, J.J., "Interior Noise Studies for General Aviation Types of Aircraft, Part I: Field Studies," *Journal of Sound and Vibration*, Vol. 58, 1978, pp. 378-390.

[4] Jha, S.K. and Catherines, J.J., "Interior Noise Studies for General Aviation Types of Aircraft, Part II: Laboratory Studies," *Journal of Sound and Vibration*, Vol. 58, 1978, pp. 391-406.

[5] Mixson, J.S., Barton, C.K., and Vaicaitis, R., "Interior Noise Analysis and Control for Light Aircraft," Paper 770445 presented at SAE Business Aircraft Meeting, Wichita, Kan., April 1976.

[6] Cockburn, J.A. and Jolly, A.C., "Structural-Acoustic Responses, Noise Transmission Losses and Interior Noise Levels of an Aircraft Fuselage Excited by Random Pressure Fields," Tech. Rept. AFFDL-TR-68-2, U.S. Air Force, Aug. 1968.

[7] Vaicaitis, R. and McDonald, W., "Noise Transmission into a Light Aircraft," AIAA Paper 78-197, AIAA 16th Aerospace Sciences Meeting, Huntsville, Ala., Jan. 16-18, 1978.

[8] Finlayson, B.A., *The Method of Weighted Residuals and Variational Principles*, Academic Press, N.Y., 1972.

[9] Craggs, A., "The Transient Response of a Coupled Plate-Acoustic System Using Plate and Acoustic Finite Elements," *Journal of Sound and Vibration*, Vol. 15, 1971, pp. 509-528.

[10] Craggs, A., "The Use of Simple Three-Dimensional Acoustic Finite Elements for Determining the Natural Modes and Frequencies of Complex Shaped Enclosures," *Journal of Sound and Vibration*, Vol. 23, 1972, pp. 331-339.

[11] Shuka, T. and Ishihara, K., "The Analysis of the Acoustic Field in Irregularly Shaped Rooms by the Finite Element Method," *Journal of Sound and Vibration*, Vol. 29, 1973, pp. 67-76.

[12] Petyt, M., Lea, J., and Koopman, G.H., "A Finite Element Method for Determining the Acoustic Modes of Irregular Shaped Cavities," *Journal of Sound and Vibration*, Vol. 45, 1976, pp. 497-502.

[13] Craggs, A., "An Acoustic Finite Element Approach for Studying Boundary Flexibility and Sound Transmission Between Irregular Enclosures," *Journal of Sound and Vibration*, Vol. 30, 1973, pp. 343-357.

[14] Nefske, D.J. and Howell, L.J., "Automobile Interior Noise Reduction Using Finite Element Methods," Paper 780365, presented at SAE Congress and Exposition, Detroit, Mich., Feb. 1978.

[15] Craggs, A., "Finite Element Method for Damped Acoustic Systems: An Application to Evaluate the Performance of Reactive Mufflers," *Journal of Sound and Vibration*, Vol. 48, 1976, pp. 377-392.

[16] Kagawa, J., Yamabsuchi, T., and Mori, A., "Finite Element Simulation of an Axisymmetric Acoustic Transmission System with a Sound Absorbing Wall," *Journal of Sound and Vibration*, Vol. 53, 1977, pp. 357-374.

[17] Joppa, P.D. and Fyte, I.M., "A Finite Element Analysis of the Impedance Properties of Irregular Shaped Cavities with Absorptive Boundaries," *Journal of Sound and Vibration*, Vol. 56, 1978, pp. 61-69.

[18] Hurty, W.C., "Dynamic Analysis of Structural Systems Using Component Modes," *AIAA Journal*, Vol. 3, April 1965, pp. 678-685.

[19] Przemieniecki, J.S., *Theory of Matrix Structural Analysis*, McGraw-Hill, N.Y., 1968.

[20] Zienkiewicz, O.C., *The Finite Element Method in Engineering Science*, McGraw-Hill, N.Y., 1968.

[21] Morse, P.M. and Ingard, K.U., *Theoretical Acoustics*, McGraw-Hill, N.Y., 1968.

[22] Karamcheti, K., *Principles of Ideal-Fluid Aerodynamics*, Wiley, N.Y., 1966.

[23] Hurty, W.C. and Rubenstein, M.F., *Dynamics of Structures*, Prentice Hall, N.J., 1964.

[24] Unruh, J.F., Scheidt, D.C., and Pomerening, D.J., "Engine Induced Structural-Borne Noise in a General Aviation Aircraft," Southwest Research Institute, San Antonio, Texas, NASA CR 159099, Aug. 1979.